JACS
JOURNAL OF THE AMERICAN CHEMICAL SOCIETY
Article
pubs.acs.org/JACS

Trapping of a Spatial Transient State During the Framework Transformation of a Porous Coordination Polymer

Mio Kondo,[†,#] Shuhei Furukawa,*[,†] Kenji Hirai,[‡] Takaaki Tsuruoka,[§] Julien Reboul,[†] Hiromitsu Uehara,[†] Stéphane Diring,[†] Yoko Sakata,[†] Osami Sakata,*[,∥] and Susumu Kitagawa*[,†,‡]

[†]Institute for Integrated Cell-Material Sciences (WPI-iCeMS), Kyoto University, Yoshida, Sakyo-ku, Kyoto 606-8501, Japan

[‡]Department of Synthetic Chemistry and Biological Chemistry, Graduate School of Engineering, Kyoto University, Katsura, Nishikyo-ku, Kyoto 615-8510, Japan

[§]Frontiers of Innovative Research in Science and Technology (FIRST), Konan University, 7-1-20, Minatojima-minamimachi, Chuo-ku, Kobe 650-0047, Japan.

[∥]Synchrotron X-ray Station at SPring-8, National Institute for Materials Science (NIMS), Kouto, Sayo, Hyogo 679-5148, Japan.

Supporting Information

ABSTRACT: Structural transformability accompanied by molecular accommodation is a distinguished feature of porous coordination polymers (PCPs) among porous materials. Conventional X-ray crystallography allows for the determination of each structural phase emerged during transformation. However, the propagation mechanism of transformation through an entire crystal still remains in question. Here we elucidate the structural nature of the spatial transient state, in which two different but correlated framework structures, an original phase and a deformed phase, simultaneously exist in one crystal. The deformed phase is distinctively generated only at the crystal surface region by introducing large guest molecules, while the remaining part of crystal containing small molecules maintains the original phase. By means of grazing incidence diffraction techniques we determine that the framework is sheared with sharing one edge of the original primitive cubic structure, leading to the formation of crystal domains with four mirror image relationships.

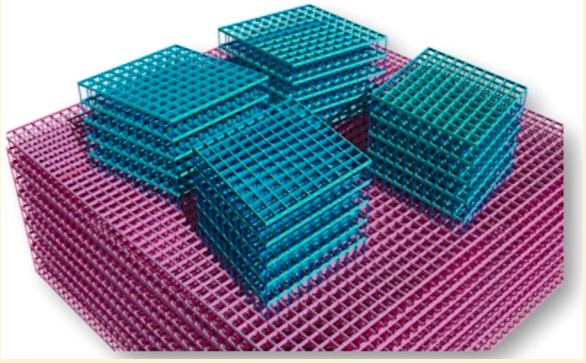

INTRODUCTION

Molecular crystalline solids that alter their structures in response to external stimuli are recognized as an intriguing class of adaptive, smart materials because the physical, chemical, or mechanical properties associated with their structures can be changed in a controlled fashion.[1,2] In addition to physical stimuli, such as light, pressure, and temperature, a chemical stimulus defined as the change of the chemical environment surrounding materials can trigger a dynamic structural transformation via molecular inclusion into solids,[3] and subsequently changing their properties, i.e., magnetism[4] or catalytic activity.[5] In particular, many studies on guest-induced structural transformation have reported the use of porous coordination polymers (PCPs),[6,7] because of the intrinsic porosity of these nanoporous crystalline materials, which enables the diffusion of molecules into an entire crystal. In addition, framework flexibility allows the optimization of their structures against molecule accommodation via relatively flexible coordination bonds.[8,9] Regarding their practical application, such flexibility is a key feature of their superb performance in storage,[10] separation,[11,12] and sensing[13] applications. However, a deeper understanding of the mechanism and dynamics involved in the guest-induced structural transformation events is required to improve those performances further.

X-ray structural analysis is a powerful method to unveil the transformation mechanism. In fact, in many reports, both framework structures of a guest-free original phase and of a guest-loaded deformed phase have been characterized using conventional single-crystal or powder X-ray diffraction measurements.[14−16] More importantly, those techniques also allowed the structural determination of a metastable state during the transformation, in which guest molecules were partially loaded into the pores of PCPs. Such detailed structural information is of high significance in tuning the characteristic sorption properties that arise from framework flexibility, such as guest selectivity, sorption hysteresis, and gate-opening behavior.[17−19] On the other hand, one should consider the correlation between the diffusion kinetics of guest molecules and the structural transformation at a given moment after environmental change before reaching equilibrium. In this snapshot, in which guest molecules become incorporated from the external PCP crystal surface, the induced structural

Received: October 7, 2013
Published: March 10, 2014

   dx.doi.org/10.1021/ja409965g | J. Am. Chem. Soc. 2014, 136, 4938−4944

transformation occurs only at the crystal surface region, whereas the remaining part of the crystal maintains the original structure. At this nonequilibrated state, or so-called spatial transient state (Scheme 1), there exist two distinct structures in one crystal: an original phase and a deformed phase. The structural elucidation of the spatial transient state and the analysis of the relationship between the original and deformed phases are of significance in the development of all porous properties related to the guest-diffusion kinetics and the structural flexibility of PCPs, e.g., separation of molecules, transportation of molecules/ions, and sensing ability.[20−22] However, the limitations of conventional X-ray diffraction techniques, in terms of the lack of spatiotemporal resolution, hinder the spatial determination of the transient state.

Scheme 1. Schematic Illustration of Spatial Transient State Observed in PCP Crystals; Once Guest Molecules Are Loaded into the System (left), the Molecules Start to Interact with Crystal Surfaces of Materials[a]

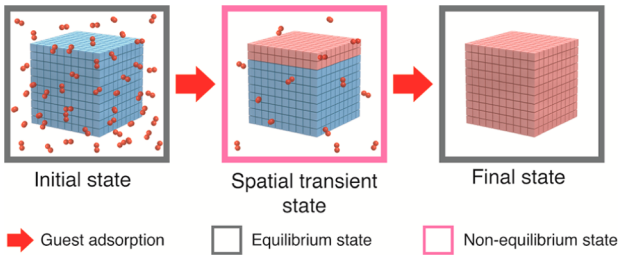

[a]Thanks to the framework flexibility, the surface region accommodating guest molecules deforms structures (the red part), whilst the remaining part still maintains the original structure (the blue part). We define this moment as a spatial transient state (middle). After reaching equilibrium, the entire structure in the crystal deforms and uniformly accommodates the molecules (right).

Here, we show that surface X-ray diffraction (grazing incident X-ray diffraction) is a new method to determine the spatial transient state. The transient state is trapped by introducing guest molecules with a size that matches the pore size exactly, which results in a slowing down of guest diffusion, thus generating a pseudo-non-equilibrated state. This partial guest incorporation only at the crystal surface region leads to heterogeneity in a PCP single crystal: a bulk phase, which maintains the initial structure, and a surface phase, which is transformed into a new deformed structure. We determine an atomic-scale in-plane structure of the surface phase and its in-plane orientation. In addition, the structural relationship between the deformed surface structure and the original bulk structure is successfully explained by an edge-shared structural transformation model within four mirror crystal domains.

EXPERIMENTAL SECTION

Materials. Reagents and solvents were purchased from commercial sources and used without further purification. Compounds **1** and BODIPY (**g**) were prepared according to literature procedures.[23,24]

Guest Exchange of 1 with g1 or g2. Single crystals of **1** were immersed into a DMF solution of **g1** or **g2** (0.1 mM) at 50 °C for 48 h. Immersed crystals were washed with fresh DMF for 10 times before measurements.

Measurement Apparatus. ^{1}H NMR, ^{13}C NMR spectra were collected with ECX400 NMR spectrometer (JEOL). UV−vis−nearIR absorption spectra were recorded with a JASCO V-670 spectrometer. Fluorescence excitation spectra were recorded with a Hitachi F-7000 fluorospectrometer. Face index of surface-modified crystals were performed with a Rigaku AFC10 diffractometer with Rigaku Saturn CCD system equipped with a rotating-anode X-ray generator producing graphite-monochromated Mo Kα radiation.

Confocal Microscopic Measurements. CLSM images of surface-modified crystals were collected on FV-1000 (Olympus), equipped with inverted optical microscope (IX-81) with objective lenses (×10, ×20, ×40, ×60 (oil-immersion lens), and ×100 (oil-immersion lens)). The samples were excited with an Ar laser (515 nm for **1⊃g1/DMF** and 488 nm for **1⊃g2/DMF**). Setting: picture size 512 × 512 pixel, emission range was 530−630 nm for **1⊃g1/DMF** and 500−600 nm for **1⊃g2/DMF**). The crystal samples were dispersed in dehydrated DMF, and the suspension was dropped on the glass plated in a sealed cell.

Polarized Fluorescent Microscopy Measurements. Polarized fluorescent microscopic images were collected on BX51 (Olympus) with objective lense (×20), equipped with Mercury lamp (U-RFL-T). The light source was polarized with U-AN360-3 and filtered using neutral density filters (U-25ND25 and U-25ND6, Olympus) and an excitation filter that had light transmission bandwidth between 530 and 550 nm (U-MWIG3, Olympus, for **1⊃g1/DMF**) or that between 470 and 495 nm (U-MNIBA, Olympus, for **1⊃g2/DMF**). The fluorescence above 575 nm (**1⊃g1/DMF**) or between 510 and 550 nm (**1⊃g2/DMF**) was detected using a CCD camera (DP72, Olympus).

SEM-EDX Measurements. Elemental analysis was performed by a JSM-7001FA field emission scanning electron microscopy operating at 15 kV, equipped with a EX-64175JMU energy-dispersive X-ray microanalyzer (JEOL).

Synchrotron X-ray Measurements for Surface Structural Analysis. Measurements were performed with a four-circle diffractometer having φ, χ, θ, and 2θ circles at beamline BL13XU for surface and interface structures, SPring-8. The desired crystal in DMF was selected just before measurement and fixed on the glass substrate with double-faced adhesive. Measurement was carried out under helium gas. In such conditions, guest DMF molecules most likely occupied the pores of the PCP crystal. The wavelength of incident X-ray was 8.00 keV (λ = 1.554 Å). Each data set was recorded using a scintillation counter.

RESULTS AND DISCUSSION

Generation of a Spatial Transient State via an Exact Size-match Strategy. A key to trapping the spatial transient state (i.e., to thus obtaining a partial guest-exchanged crystal only at the crystal surface region) is to slow down the diffusion kinetics of guest molecules in the pores. Our strategy consisted of choosing a host−guest system with a strong interaction based on an exact size-match between the pore size of the host framework and the size of the guest molecule. In such a system, guest molecules should pass through highly crowded channels, which would prevent the rapid diffusion into an entire crystal. A tetragonal framework, $[Zn_2(ndc)_2(dabco)]_n$ (**1**), (ndc = 1,4-naphthalenedicarboxylate, dabco = 1,4-diazabicyclo[2.2.2]-octane), in which two-dimensional (2D) square grids constructed by zinc paddlewheel units and ndc molecules are pillared by dabco molecules,[25,26] was selected as a host PCP system (Figure 1a and b). This was because of its remarkable single crystallinity, which is essential to determine a surface crystal structure using synchrotron grazing incident X-ray diffraction. We chose boron dipyrromethene (BODIPY) derivatives[27,28] (Figure 1c and d) as guest candidates because their high fluorescent quantum yields allow us to characterize the spatial heterogeneity of guest molecule distribution using fluorescence microscopy.

Note that **1** possesses one-dimensional channels along the *c* axis and its entrance size varies depending on the orientation of the naphthalene ring, because 1,4-ndc rotates freely along the

dx.doi.org/10.1021/ja409965g | J. Am. Chem. Soc. 2014, 136, 4938−4944

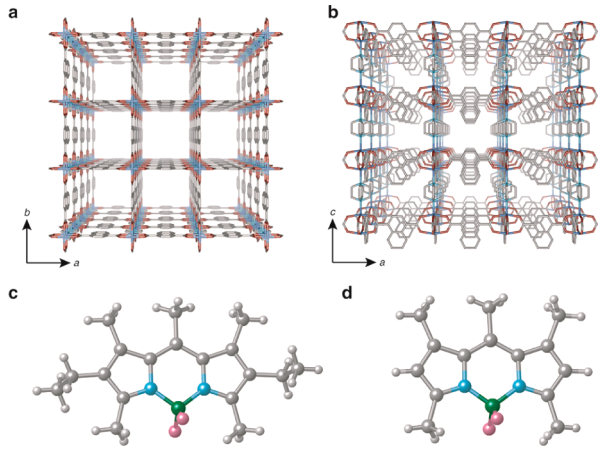

Figure 1. The structures of the zinc framework, $[Zn_2(ndc)_2(dabco)]_n$ (**1**) with maximal pore entrance size along the (a) ⟨001⟩ and (b) ⟨100⟩ axes. Hydrogen atoms and guest molecules are omitted for clarity. The π-plane of naphthalene rings is aligned parallel to the ⟨001⟩ axis to make the size of pore entrance maximum. Molecular structures of (c) **g1** and (d) **g2**.

axis of the 1,4 position even in the crystalline state. The maximal entrance size was estimated as 7.9 × 7.9 Å^2, assuming that all naphthalene rings are parallel to the *c* axis[29] (Figure 1). The guest molecules employed in our experiment were designed to have a molecular size (**g1**: 5.6 × 8.7 × 15.0 Å^3)[29] that is similar to the maximal entrance size to slow down the diffusion of guest molecules.

The incorporation of guest molecules was achieved by the immersion of as-synthesized single crystals of **1⊃DMF** (**1**·3DMF·2H_2O) into the DMF solution of the BODIPY molecule (**g1**) at 50 °C for 2 days. Single crystals of **1** have a rectangular crystal morphology in which four surfaces are parallel to the channels (denoted as the {100} surfaces) and the other two surfaces are perpendicular to the channels (denoted as the {001} surfaces). Because of the one-dimensional nature of the pores, the incorporation of guest molecules should occur only at the interfaces of the {001} crystal surfaces, as shown in Figure 2. In fact, the confocal laser scanning microscopy (CLSM) images (Figure 2c) of the crystal after treatment with the BODIPY molecules indicated that only two crystal surfaces exhibited strong fluorescence after excitation at 515 nm. The fluorescence spectrum obtained under the CLSM condition corresponded to that of **g1** in DMF solution (Figure S1 in the SI), which suggests that the BODIPY molecules were incorporated into the pores. A face index analysis performed using a single-crystal X-ray diffractometer for the same crystal successfully assigned the two surfaces with fluorescence to the {001} surfaces. Because we were not able to determine the diffusion distance of BODIPY by CLSM due to its limited spatial resolution, we performed SEM-EDX measurements. Using the F atoms of BODIPY as an elemental probe, the travel distance was roughly estimated to be 0.5−1 μm (Figure 3). Note that the longer immersion time of **1⊃DMF** into the BODIPY solution (for 1 week) did not yield a significant difference. The results of all experiments imply that the BODIPY molecules are incorporated into the channel only at the {001} crystal interfaces, and that the diffusion along the pores becomes very slow and is restricted in the crystal surface region by the strong confinement effect of PCPs. Thus, we obtained the spatial transient state as the pseudo-non-

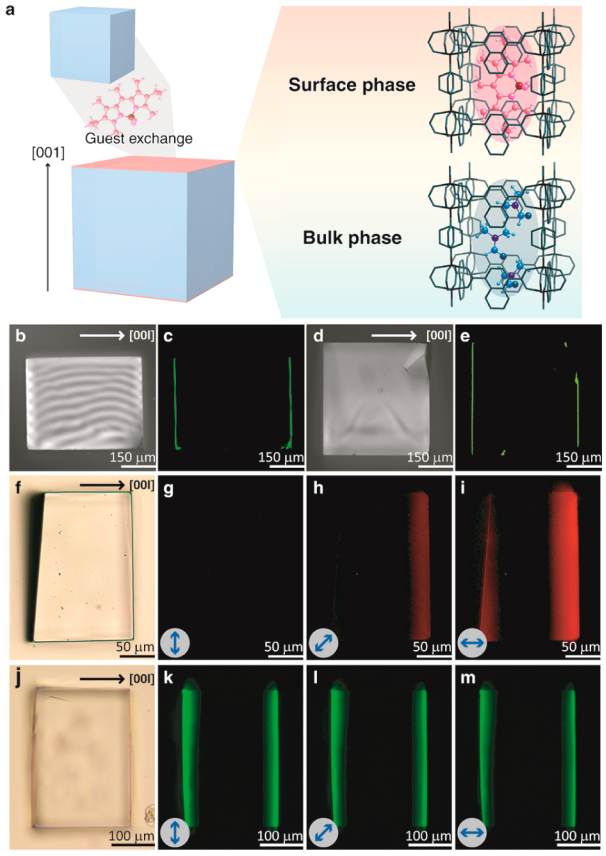

Figure 2. (a) Schematic illustration of trapping of spatial transient state in **1⊃g1/DMF**. (b) Transmission and (c) CLSM images of **1⊃g1/DMF**. (d) Transmission and (e) CLSM images of **1⊃g2/DMF**. (f) Transmission and (g−i) polarized fluorescent microscope images of **1⊃g1/DMF**. (j) Transmission and (k−m) polarized fluorescent microscope images of **1⊃g2/DMF**. Blue arrows indicate the direction of polarization of excitation light. For polarized fluorescent microscope images, the fluorescence above 575 nm (**1⊃g1/DMF**) or between 510 and 550 nm (**1⊃g2/DMF**) was detected.

equilibrated state with spatial heterogeneity of guest−molecule distribution (**1⊃g1/DMF**): the bulk phase, which accommodated DMF molecules, and the surface phase, which accommodated the BODIPY molecules.

To gain insight into the confinement effect of the pores, we performed polarized fluorescence microscopy measurements of **1⊃BODIPY/DMF**, in which the excitation light was linearly polarized using a polarizing plate, and emission was recorded without polarization. Crystals at the spatial transient state with the smaller BODIPY derivative (**g2**: 4.8 × 8.6 × 10.6 Å^3, see Figure 1d) were also used as a reference. There was no significant difference between **1⊃g1/DMF** and **1⊃g2/DMF** in the CLSM study, whereas the polarized fluorescent microscopy clearly unveiled a difference in confinement between **g1** and **g2**. In the case of **g1**, which has a slightly longer molecular length than **g2** because of the ethyl groups introduced into the pyrrole core, the strongest fluorescence was observed when the excitation light was polarized along the *c* axis (Figure 2i) and no florescence was observed when the excitation light was polarized perpendicular to the *c* axis (Figure 2g). Because the direction of the transition dipole moment of BODIPY derivatives corresponds to the longer molecular axis,[30] these results suggest that the **g1** molecules are strongly confined to aligning themselves in the one-dimensional pores and that

dx.doi.org/10.1021/ja409965g | J. Am. Chem. Soc. 2014, 136, 4938−4944

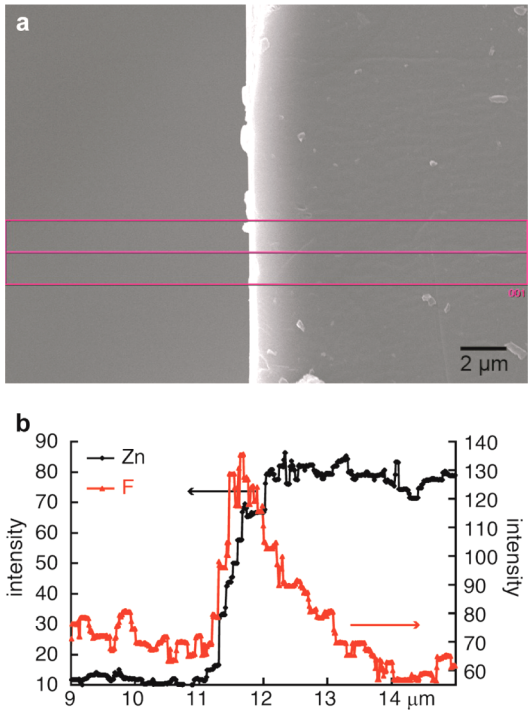

Figure 3. (a) SEM image of **1⊃g1/DMF**. (b) Line scan of Zn and F of **1⊃g1/DMF**, which were performed at line displayed in SEM image. Acceleration voltage was 15 kV.

molecular movements, such as rotation, are restricted. In contrast, a clear polarization effect was not observed for **1⊃g2/DMF** (Figures 2k–m and 4). Because of the shorter molecular

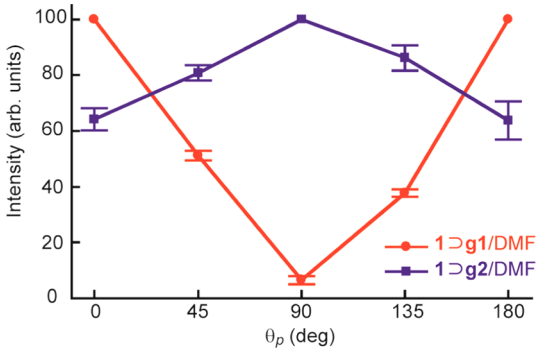

Figure 4. Change of fluorescent intensity of **1⊃g1/DMF** (red line) and **1⊃g2/DMF** (blue line) at various polarization angles (θ_p).

length of **g2** and the rotation of the naphthalene moiety, two kinds of arrangements that were almost orthogonal with each other can be formed (Figure S2 in the SI). Therefore, **g2** absorbed excitation light regardless of the polarization angle.

Structural Determination of the Deformed Surface Phase. The series of tetragonal frameworks based on the zinc paddlewheel units display a shearing–type structural deformation in response to molecule accommodation.[18,25,31] A similar structural transformation of the surface phase can be anticipated because this dynamic nature definitely contributes to the strong confinement of the **g1** molecules in the surface phase. However, conventional single-crystal or powder X-ray diffraction measurements did not allow the structural investigation of the surface phase; rather, they only provided the diffractions from the bulk phase, which maintained its original structure (Figure S3 in the SI). This was because, during these measurements, the contribution of the surface phase (less than 1 μm in thickness) became negligible compared with that of the remaining bulk phase.

To elucidate the structure of the surface phase, we attempted to perform synchrotron grazing incidence X-ray diffraction, which allows the detection of a faint–intensity signal from a crystalline surface because of the shallow penetration of X-rays (Figure 5). A crystal of **1⊃g1/DMF** with a size greater than 100

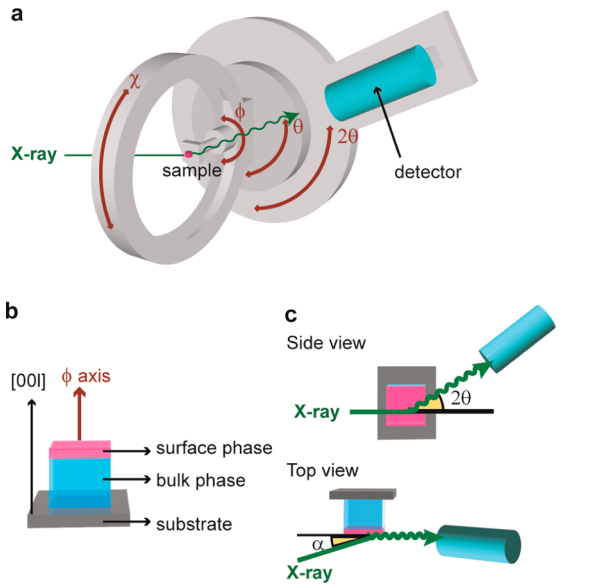

Figure 5. (a) Schematic drawing of the four-circle diffractometer at beamline BL13XU for surface and interface structures, SPring-8. For ϕ scans, θ–2θ angles were fixed to each Bragg position, and only ϕ angles were rotated to determine the orientation of crystal domains. (b) The schematic drawing of the crystal of **1⊃g1/DMF** fixed on the glass substrate. The orientation of the crystal was determined by out-of-plane measurements. (c) The direction of the incident X-ray beam in in-plane measurements.

μm was fixed on a glass substrate in the ⟨001⟩ direction, perpendicular to the substrate (Figure 5b and Figure S4 in the SI), and diffraction intensities were recorded using an X-ray beam with a size of 50 × 50 μm^2. Note that the *ab* plane of the bulk phase was parallel to the substrate, and diffractions with the indices of (*hk*0) were detectable in in-plane measurement. By careful scanning around the 100 or 010 Bragg positions of the bulk phase, we detected diffractions with two different 2θ values ($2\theta_{100}$ = 8.18 and $2\theta'_{100}$ = 8.24°). To assign these diffractions, diffraction intensities at various X-ray incident angles (α) were measured (Figure 5c). As shown in Table 1, the ratio of intensity between these diffractions ($2\theta'_{100}/2\theta_{100}$) increased with decreasing X-ray incident angles. The smaller incident angle leads to the enhancement of the signals from the surface because of the shallower penetration depth of the X-ray

Table 1. Intensity of θ_{100} and θ'_{100} at Various Grazing Incident Angles (α)

α	$I(2\theta_{100})$/cps	$I(2\theta'_{100})$/cps	$I(2\theta'_{100})/I(2\theta_{100})$
0.05	9000	18000	2.00
0.10	18000	35000	1.94
0.15	9000	8200	0.91
0.20	835	200	0.24

dx.doi.org/10.1021/ja409965g | J. Am. Chem. Soc. 2014, 136, 4938–4944

beam. Therefore, this observation suggests that the diffraction with $2\theta'_{100}$ originates from the surface phase and the diffraction with $2\theta_{100}$ originates from the bulk phase. Similarly, diffraction peaks with three different 2θ values ($2\theta_{110}$ = 11.58, $2\theta'_{110}$ = 11.26 and $2\theta''_{110}$ = 12.07°) were observed around the 110 and 1−10 Bragg positions of the bulk phase. Because the in-plane (grazing incidence) measurement for the host crystal of **1⊃DMF** gave only a diffraction with one 2θ value (11.61°), the diffraction with $2\theta_{110}$ (11.58°) can be assigned to the 110 Bragg peak from the bulk phase. The remaining new diffractions with $2\theta'_{110}$ and $2\theta''_{110}$ values have originated from the surface phase. Note that the 4-fold symmetry of the structure based on a tetragonal crystal system affords the same 2θ values between the (100) and (010) diffractions and between the (110) and (1−10) diffractions for the bulk phase.

On the basis of the 2θ values obtained via the in-plane diffraction measurement, we constructed a plausible structural model for the surface phase along the *ab* plane. First, a single unit cell of the surface phase in the *ab* plane should shear from a square to a rhombus, in which the lengths of the four sides are identical. For this rhombic-shaped unit cell, only one 2θ value for the 100 or 010 Bragg peaks should be observed because the *d*-spacing of the (100) and (010) planes are identical (Figure 6a). In contrast, because of the distinct *d*-spacing values for the (110) and (1−10) planes, the 2θ values should be different between the 110 and 1−10 Bragg peaks (Figure 6b).

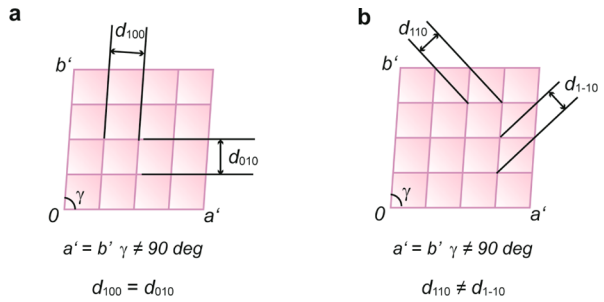

Figure 6. Schematic illustrations for *d*-spacing of (100) and (010) (a) and that of (110) and (1−10) (b) for a rhombic shaped cell.

As summarized in Table 2, only one 2θ value for the 100 Bragg peak was observed for the surface phase ($2\theta'_{100}$, now denoted as $2\theta_{100}$(S)) and two different 2θ values, of 11.26 and 12.07 degrees, were observed in the surface phase, which can be assigned to the 110 and 1−10 Bragg peaks ($2\theta'_{110}$ and $2\theta''_{110}$, now denoted as $2\theta_{110}$(S) and $2\theta_{1-10}$(S), respectively).

Table 2. Summary of 2θ Values of the Bulk and the Surface Phases of 1⊃g1/DMF Obtained from in-Plane Measurement

	index	phase	2θ values/deg
$2\theta_{100}$	100	bulk	8.18
$2\theta_{100}$(S)	100	surface	8.24
$2\theta_{110}$	110	bulk	11.58
$2\theta_{110}$(S)	110	surface	11.26
$2\theta_{1-10}$(S)	1−10	surface	12.07

Second, the angle γ of its rhombus cross section was estimated to be 86° from the 2θ values of $2\theta_{110}$(S) and $2\theta_{1-10}$(S) (Figure S5 and eq S1 in the SI), and the length of the sides of the rhombus in the surface phase was almost identical to that of the square in the bulk phase, which were estimated from the angle γ, $2\theta_{100}$, and $2\theta_{100}$(S) (Figure S5 and eq S2 in the SI). Therefore, the dynamics of the phase transformation can be represented by just one degree of freedom, the angle γ, as shown in Figure 7a and b.

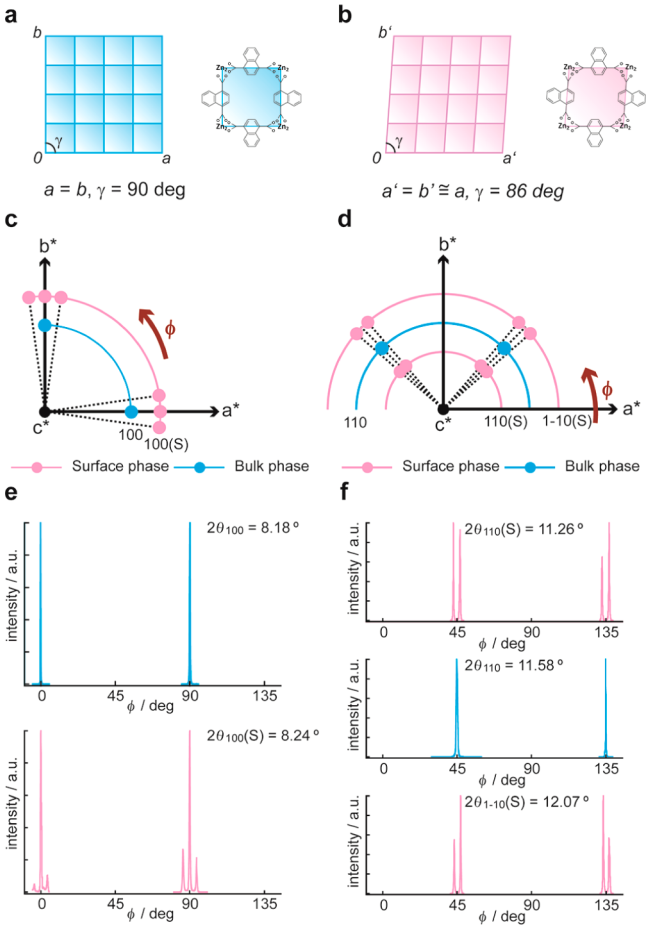

Figure 7. (a) Schematic illustration of unit cell along *ab* plane of the bulk phase. (b) Schematic illustration of unit cell along *ab* plane of the surface phase. The reciprocal lattice space corresponding to the rotational scan around the [001] direction for (c) 100 and 010 and (d) 110 and 1−10 diffractions. The results of ϕ scans at (e) 100 and 010 and (f) 110 and 1−10. Blue and red lines indicate the diffraction from the bulk and the surface phase, respectively.

Elucidation of the Structural Relationship between the Deformed Surface Phase and the Original Bulk Phase. To assess the propagation of structural transformations in the crystal, the structural relationship between the deformed surface phase and the original bulk phase in the atomic scale was determined. The scan of the rotation angle around the [001] direction (the ϕ scan) of each Bragg peak was performed. In this measurement, angles between the incident X-ray and the diffractometer ($2\theta_d$) were fixed to the 2θ values of desired Bragg peaks: for instance, $2\theta_d$ was fixed to $2\theta_{100}$ (8.18°) to perform the ϕ scan of 100 diffraction for the bulk phase. Upon rotation of the ϕ angle, the desired diffraction is observable only when the crystal satisfies Bragg's law (Figure S6 in the SI). Therefore, the orientation of the crystal in the in-plane direction is determined. First, a ϕ scan against the 100 and 110 diffractions of the bulk phase was performed. Both the 100 and 110 Bragg peaks of the bulk phase were observed periodically every 90° as singlet peaks, indicating that the bulk

dx.doi.org/10.1021/ja409965g | J. Am. Chem. Soc. 2014, 136, 4938−4944

phase maintains its single crystallinity. In contrast, the splitting of the peak was observed for all 100 (triplet), 110 (doublet), and 1−10 (doublet) Bragg peaks of the surface phase, whereas the center of each doublet or triplet peak was located at exactly the same ϕ angle as the corresponding peak of the bulk phase (Figure 7c−f, Tables 3 and 4).

Table 3. Summary of in-Plane Measurement for 100 Bragg Peaks

	bulk		surface		
index	2θ	ϕ	2θ	ϕ	$\Delta\phi$
1 0 0	8.18	0	8.25	−4	−4
				0	0
				4	4
	8.18	90	8.24	86	−4
				90	0
				94	4
	–	180	8.24	176	−4
				180	0
				184	4
	8.18	270	8.24	266	−4
				270	0
				274	4

Table 4. Summary of in-Plane Measurement for 110 and 1-10 Bragg Peaks

	bulk		surface		
index	2θ	ϕ	2θ	ϕ	$\Delta\phi$
1 1 0	11.58	45	11.26	43	−2
				47	2
	11.58	135	11.25	133	−2
				137	2
1 −1 0	11.58	45	12.07	43	−2
				47	2
	11.58	135	12.07	133	−2
				137	2

The variation of ϕ angles at the surface phase was interpreted by assuming an edge-shared structural transformation model with the generation of four mirror domains (Figure 8). The transformation from the square to the rhombus (i.e., the change of γ from 90 to 86°) is supposed to occur with partial maintenance of the connectivity at the interface between the surface phase and the bulk phase; i.e., one out of the four edges of the rhombus in the surface phase should maintain its original position, leading to the formation of four kinds of crystal domains originated from a thermodynamically equivalent shearing motion. On the basis of the surface model described above, the difference in the ϕ angle between the bulk phase and the surface phase ($\Delta\phi$) was calculated to be $-90 + \gamma$, 0 or $90 - \gamma$ ° for the 100 Bragg peaks and $-45 + 0.5\gamma$ or $45 - 0.5\gamma$ ° for the 110 and 1−10 Bragg peaks, respectively. These calculated values are in excellent agreement with the observed $\Delta\phi$ values as shown in Tables 3 and 4. These observations indicate that the directional distortion in the surface phase upon transition is restricted by the connection with the bulk phase.

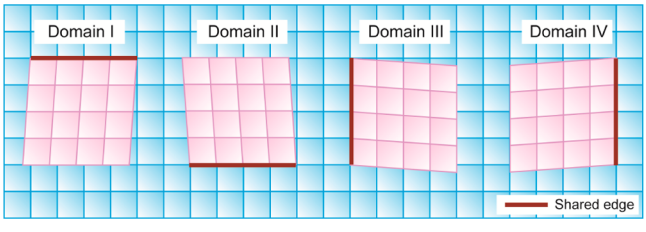

Figure 8. Schematic model of the structural relationship between the surface and the bulk phases on the (001) surface. Red lines indicate the edges that maintain the original position upon crystal transformation to the surface phase. Four mirror domains of the surface phase were formed, depending on the direction of shearing motion.

CONCLUSIONS

The results presented here showed, for the first time, the structural analysis of PCP crystals, which were in the spatial transient state of the structural transformation (**1⊃g1/DMF**) as assessed on the basis of synchrotron grazing incidence diffraction measurements. **1⊃g1/DMF** exhibited a heterostructure that was composed of the bulk and the surface phase because of the slow diffusion of **g1** into the pores, and the structural transformation from **1⊃DMF** to **1⊃g1/DMF** was accompanied by the sharing of one out of four edges of the crystal cell to maintain the connectivity between the two phases. The results demonstrated clearly that the spatial orientation of the crystal phase after the transformation should be regulated by the structure of the original phase in some cases. Recently, several reports demonstrated unexpected sorption properties that could not be explained by the local chemical structure or by the pore surface functionality; rather, they may be attributed to mesoscopic crystalline defects such as crystal domain formation or unknown surface structures.[20−22] However, although the origin of such phenomena has not been determined structurally, it has been discussed phenomenologically. The results presented here regarding the spatial transient state will definitely provide a new insight into the interpretation of these phenomena, because the information obtained using this system, such as the propagation of structural transformation and the domain formation, is strongly correlated with the diffusion of molecules. The next stage of this research is the determination of the transformation mechanism under a controlled vapor atmosphere using surface X-ray diffraction.

ASSOCIATED CONTENT

Supporting Information

Fluorescence spectra, summary of polarized fluorescent microscopy, additional structure figures, PXRD, and additional figures for surface X-ray diffraction measurements. This material is available free of charge via the Internet at http://pubs.acs.org.

AUTHOR INFORMATION

Corresponding Authors

shuhei.furukawa@icems.kyoto-u.ac.jp (S.F.)
Sakata.Osami@nims.go.jp (O.S.)
kitagawa@icems.kyoto-u.ac.jp (S.K.)

Present Address

[#]Department of Life and Coordination-Complex Molecular Science, Institute for Molecular Science, Higashiyama 5-1, Myodaiji, Okazaki, Aichi 444-8787, Japan.

Notes

The authors declare no competing financial interest.

■ ACKNOWLEDGMENTS

M.K. is grateful to JSPS Research Fellowships for Young Scientists. This work was supported by ERATO "Kitagawa Integrated Pores Project" of Japan Science and Technology Agency (JST). The synchrotron X-ray experiments were performed at BL13XU in the SPring-8 with the approval of the JASRI (Proposal No. 2010A1393). We acknowledge Prof. Kensuke Akamatsu and Prof. Hidemi Nawafune for the helpful advice on the SEM-EDX measurement. iCeMS is supported by World Premier International Research Initiative (WPI), MEXT, Japan.

■ REFERENCES

(1) Chollet, M.; Guerin, L.; Uchida, N.; Fukaya, S.; Shimoda, H.; Ishikawa, T.; Matsuda, K.; Hasegawa, T.; Ota, A.; Yamochi, H.; Saito, G.; Tazaki, R.; Adachi, S.; Koshihara, S. *Science* **2005**, *307*, 86−89.
(2) Kobatake, S.; Takami, S.; Muto, H.; Ishikawa, T.; Irie, M. *Nature* **2007**, *446*, 778−781.
(3) Atwood, J. L.; Barbour, L.J.; Jerga, A.; Schottel, B. L. *Science* **2002**, *298*, 1000−1002.
(4) Coronado, E.; Gimenez-Marques, M.; Espallargas, G. M.; Brammer, L. *Nat. Commun.* **2012**, *3*, 828.
(5) Huang, Z.; White, P. S.; Brookhart, M. *Nature* **2010**, *465*, 598−601.
(6) Yaghi, O. M.; O'Keeffe, M.; Ockwig, N. W.; Chae, H. K.; Eddaoudi, M.; Kim, J. *Nature* **2003**, *423*, 705−714.
(7) Kitagawa, S.; Kitaura, R.; Noro, S. *Angew. Chem., Int. Ed.* **2004**, *43*, 2334−2375.
(8) Férey, G. *Chem. Soc. Rev.* **2009**, *37*, 191−214.
(9) Horike, S.; Shimomura, S.; Kitagawa, S. *Nat. Chem.* **2009**, *1*, 695−704.
(10) Rabone, J.; Yue, Y.-F.; Chong, S. Y.; Stylianou, K. C.; Bacsa, J.; Bradshaw, D.; Darling, G. R.; Berry, N. G.; Khimyak, Y. Z.; Ganin, A. Y.; Wiper, P.; Claridge, J. B.; Rosseinsky, M. J. *Science* **2010**, *329*, 1053−1057.
(11) Xiao, B.; Byrne, P. J.; Wheatley, P. S.; Wragg, D. S.; Zhao, X.; Fletcher, A. J.; Thomas, K. M.; Peters, L.; Evans, J. S. O.; Warren, J. E.; Zhou, W.; Morris, R. E. *Nat. Chem.* **2009**, *1*, 289−294.
(12) Shimomura, S.; Higuchi, M.; Matsuda, R.; Yoneda, K.; Hijikata, Y.; Kubota, Y.; Mita, Y.; Kim, J.; Takata, M.; Kitagawa, S. *Nat. Chem.* **2010**, *2*, 633−637.
(13) Takashima, Y.; Martínez, V. M.; Furukawa, S.; Kondo, M.; Shimomura, S.; Uehara, H.; Nakahama, M.; Sugimoto, K.; Kitagawa, S. *Nat. Commun.* **2011**, *2*, 168.
(14) Lee, E. Y.; Suh, M. P. *Angew. Chem., Int. Ed.* **2004**, *43*, 2798−2801.
(15) Matsuda, R.; Kitaura, R.; Kitagawa, S.; Kubota, Y.; Belosludov, R. V.; Kobayashi, T. C.; Sakamoto, H.; Chiba, T.; Takata, M.; Kawazoe, Y.; Mita, Y. *Nature* **2005**, *436*, 238−241.
(16) Kubota, Y.; Takata, M.; Matsuda, R.; Kitaura, R.; Kitagawa, S.; Kobayashi, T. C. *Angew. Chem., Int. Ed.* **2006**, *45*, 4932−4936.
(17) Chandler, B. D.; Enright, G. D.; Pawsey, S.; Ripmeester, J. A.; Cramb, D. T.; Shimizu, G. K. H. *Nat. Mater.* **2008**, *7*, 229−235.
(18) Seo, J.; Matsuda, R.; Sakamoto, H.; Bonneau, C.; Kitagawa, S. *J. Am. Chem. Soc.* **2009**, *131*, 12792−12800.
(19) Serre, C.; Mellot-Draznieks, C.; Surble, S.; Audebrand, N.; Filinchuk, Y.; Férey, G. *Science* **2007**, *315*, 1828−1831.
(20) Matsuda, R.; Tsujino, T.; Sato, H.; Kubota, Y.; Morishige, K.; Takata, M.; Kitagawa, S. *Chem. Sci.* **2010**, *1*, 315−321.
(21) Sholl, D. S. *Nat. Chem.* **2011**, *3*, 429−430.
(22) Hibbe, F.; Chmelik, C.; Heinke, L.; Pramanik, S.; Li, J.; Ruthven, D. M.; Tzoulaki, D.; Kärger, J. *J. Am. Chem. Soc.* **2011**, *133*, 2804−2807.
(23) Guo, B.; Peng, X.; Cui, A.; Wu, Y.; Tian, M.; Zhang, L.; Chen, X.; Gao, Y. *Dyes Pigm.* **2007**, *73*, 206−210.
(24) Goeb, S.; Ziessel, R. *Tetrahedron Lett.* **2008**, *49*, 2569−2574.
(25) Dybtsev, D. N.; Chun, H.; Kim, K. *Angew. Chem., Int. Ed.*, **2004**, *43*, 5033-5036 (2004).
(26) Chun, H.; Dybtsev, D. N.; Kim, H.; Kim, K. *Chem.—Eur. J.* **2005**, *11*, 3521−3529.
(27) Loudet, A.; Burgess, K. *Chem. Rev.* **2007**, *107*, 4891−4932.
(28) Ulrich, G.; Ziessel, R.; Harriman, A. *Angew. Chem., Int. Ed.* **2008**, *47*, 1184−1201.
(29) The pore sizes of the framework (**1**) and the sizes of guest molecules (**g1** and **g2**) were estimated by considering van der Waals' radii of constituent atoms. For **1**, naphthalene rings in the crystal structure of **1**⊃ **DMF** were rotated to make all rings parallel to the *c* axis. The structures of **g1** and **g2** were obtained from the results of single-crystal X-ray analysis.
(30) Kim, T. G.; Castro, J. C.; Loudet, A.; Jiao, J. G.-S.; Hochstrasser, R. M.; Burgess, K.; Topp, M. R. *J. Phys. Chem. A* **2005**, *110*, 20−27.
(31) Chen, B.; Liang, C.; Yang, J.; Contreras, D. S.; Clancy, Y. L.; Lobkovsky, E. B.; Yaghi, O. M.; Dai, S. *Angew. Chem., Int. Ed.* **2006**, *45*, 1390−1393.